



Traversing the nucleation-growth landscape through heterogeneous random walksKaicheng Zhu ¹ and Haibin Su ^{1,2,*}¹*Department of Chemistry, The Hong Kong University of Science and Technology, Kowloon, Hong Kong*²*HKUST Shenzhen-Hong Kong Collaborative Innovation Research Institute, Futian, Shenzhen 518048, China*

(Received 25 January 2023; revised 20 April 2023; accepted 18 May 2023; published 8 June 2023)

The nucleation-growth process is a crucial component of crystallization. While previous theoretical models have focused on nucleation events and postnucleation growth, such as the classical nucleation theory and Lifshitz-Slyozov-Wagner model, recent advancements in experiments and simulations have highlighted the inability of classical models to explain the transient dynamics during the early development of nanocrystals. To address these shortcomings, we present a model that describes the nucleation-growth dynamics of individual nanocrystals as a series of reversible chain reactions, with the free energy landscape extended to include activation-adsorption-relaxation reaction pathways. By using the Monte Carlo method based on the transition state theory, we simulate the crystallization dynamics. We derive a Fokker-Planck formalism from the master equation to describe the nucleation-growth process as a heterogeneous random walk on the extended free energy landscape with activated states. Our results reveal the transient quasiequilibrium of the prenucleation stage before nucleation starts, and we identify a postnucleation crossover regime where the dynamic growth exponents asymptotically converge towards classical limits. Additionally, we generalize the power laws to address the dimension and scale effects for the growth of large crystals.

DOI: [10.1103/PhysRevE.107.064110](https://doi.org/10.1103/PhysRevE.107.064110)**I. INTRODUCTION**

The nucleation-growth process plays a pivotal role in the intricate nonequilibrium dynamic phase transitions in condensed matter systems [1–3]. The two-stage process of nucleation and growth elucidates the emergence of a new phase, wherein small nuclei form due to fluctuations, followed by their successive growth driven by thermodynamic forces. The occurrence of crystal growth via an intermediate polymorph that is not thermodynamically preferred is commonly referred to as Ostwald's ripening, in the context of crystallization [4–6]. The Wilson-Frenkel model provided a succinct elucidation of the nucleation rate, hinging on the free energy of the critical nucleus [7,8]. This model was further extended by computing the critical value from a free energy profile that incorporated both bulk energy and interfacial interactions [9]. Notably, Becker and Doring (BD) developed a kinetic model that utilized ordinary differential equations to describe Ostwald's ripening [10]. Lifshitz, Slyozov, and Wagner (LSW) subsequently derived growth exponents of 1/2 and 1/3 for the reaction and diffusion limits, respectively, under flux-balance conditions [11,12]. Later research demonstrated that the long-time behavior of the BD model was in agreement with the diffusion-limited scenario of the LSW model [13–15]. Despite the initial triumph of classical models, modern studies have revealed unprecedented phenomena that transcend the conventional scope of these early theories.

Recent simulations and experiments have demonstrated that the Wilson-Frenkel model is inadequate for providing a

quantitative explanation of crystal growth kinetics [16–18]. For instance, the important role played by the structural order in the nucleation-growth dynamics was reported by simulations [19,20]. Different power-law relations that cannot be accounted for by the LSW model were characterized by time-resolved measurements of nanoparticle crystallization, where continuous transitions across different growth regimes were also observed [21–23]. A multistep process in which nanocrystal growth was coupled with transient structural reorganization was observed in liquid-cell transmission electron microscopy experiments [24–27]. Utilizing super-resolution techniques, researchers have further elucidated the structural reordering during the prenucleation stage at atomic scale resolutions [28,29]. These emergent phenomena have prompted significant theoretical advancements aimed at explaining the physicochemical mechanism of microscopic crystallization, particularly during the early stages of nanocrystal development.

Here we report a theoretical work that delineates the evolution of individual nanocrystals through a series of intricately linked chain reactions. This work captures the reaction mechanism via the activation-adsorption-relaxation pathway of a single-particle exchange event. Utilizing the transition state theory, we calculate the activation energy and perform Monte Carlo simulations (MCSs) to showcase the stochastic reaction dynamics throughout both the prenucleation and postnucleation stages. We describe the evolution of the probability density function through the master equation (ME), solving it in a continuous-time fashion. Additionally, we establish that the nucleation-growth dynamics can be characterized as a generalized heterogeneous random walk on the activated free energy landscape, with the Fokker-Planck equation (FPE)

*Corresponding author: haibinsu@ust.hk

derived from the ME. This finding contrasts with previous works on anomalous diffusion processes in real space [30–34]. Our mathematical derivations provide quantitative relationships for the different transient regimes of the nucleation-growth process. In the prenucleation stage, the system reaches a transient quasiequilibrium state following initial crystallization. After nucleation events, the nanocrystal experiences rapid growth before the long-time linear-growth regime. Finally, we present generalized characteristic growth exponents that account for the dimension and scale effects observed during the late-stage growth of large nanocrystals.

II. MODEL AND RESULTS

A. Reaction mechanism and activation-adsorption-relaxation pathway

In the context of developing a single nanocrystal, the local system constitutes a biphasic mixture comprising a liquid solution, where solute particles dissolve homogeneously in the solvent, along with a solid multiparticle crystalline cluster. To simplify matters and ensure generality, we model the solute particles as identical particles, irrespective of the specific type of solution, be it ionic or molecular. The total free energy of this system comprises three extensive components: (1) the bulk free energy of the solution, (2) the bulk free energy of the crystal, and (3) the surface free energy of the solution-crystal interface. In an open system linked to an ideal constant bath, the solution remains fixed and is deemed to be an implicit background reference. Therefore, its free energy is not explicit. Owing to the extensive nature of the interfacial free energy, the ground-state condition necessitates that the area of the solution-crystal surface be minimized. As a result, the ground-state free energy of such a system in three dimensions is expressed as follows:

$$G(n) = 4a\pi r^2(n) + bV_0n, \quad (1)$$

where n is the number of particles in the crystalline cluster, a and b are the interface and bulk free energy density respectively, $r(n) = \sqrt[3]{3V_0n/4\pi}$ is the crystal radius, and V_0 is the volume of a single particle. In this paper, we set V_0 as the unit volume so that n plays the role of the normalized crystal volume. In crystallization, $a > 0$ and $b < 0$, as $4a\pi r^2(n)$ and bV_0n contribute to the driving forces for solvation and crystallization respectively. The total free energy G , as the sum of these components, reaches a global maximum when $n = n_c$. When $n < n_c$, the growth of crystal is thermodynamically unfavored, but when $n > n_c$, the crystal growth is favored by the net thermodynamic force.

The evolution of an individual nanocrystal is modeled as a series of reversible chain reactions where the elementary event is the single-particle exchange between the solution and crystal phases and no multicrystal coalescence is taken into account [Fig. 1(a)]. The reaction mechanism is demonstrated through an activation-adsorption-relaxation pathway, as an analog of Marcus theory of electron transfer [35,36]. Each particle-exchange event consists of three transient steps: (1) an activation step from the initial ground state to the preadsorption activated state, driven by thermal fluctuation; (2) a fast adsorption step from the pre- to the postadsorption activated state, as a single particle hops across the solution-

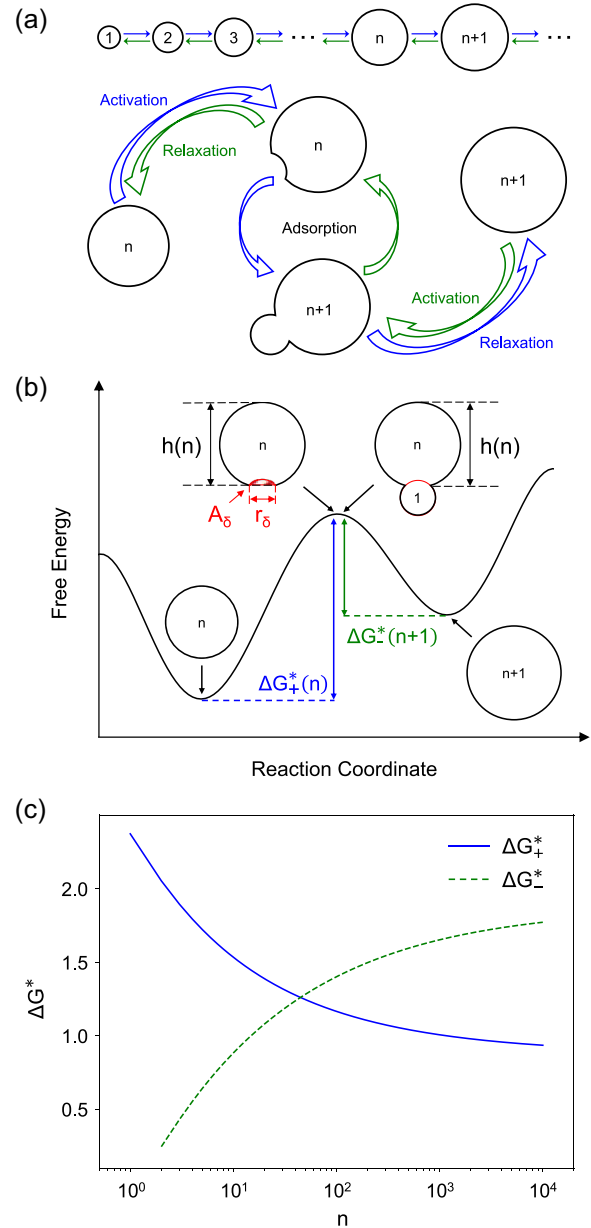


FIG. 1. Reaction mechanism and free energy profiles of activation energies. (a) The scheme of the chain reactions and the activation-adsorption-relaxation pathway of crystallization. n denotes the normalized crystal volume. (b) The free energy profile along the reaction pathway, when $n < n_c$. ΔG_{\pm}^* is the forward or backward activation energy. The activated conformations are in the shapes of lune and gourd. (c) The size-dependent activation energy. At n_c , $\Delta G_+^* = \Delta G_-^*$.

crystal interface; (3) a relaxation step from the postadsorption activated state to the final ground state. Since the adsorption is completed instantaneously, it is an infinitely small step on the reaction pathway, so that the free energies of the pre- and postadsorption activated states are the same. According to the transition state theory, the energy of the activated states is the maximum on the minimum-energy pathway, as the saddle point on the potential energy surface. In a forward reaction where $n \rightarrow n + 1$ as shown in Fig. 1(b), the preadsorption

activated crystal is in the shape of a lune, i.e., a relative complement of a single particle in the crystal ball, and the postadsorption activated crystal is the shape of a gourd, i.e., a union of a single particle and the crystal ball. These distorted conformations exhibit the facilitating role of surface defects as the extension of the nucleation sites in heterogeneous nucleation. Because they have the same free energy, the area of the red-shaded spherical cap in Fig. 1(b) is determined as follows:

$$A_\delta = \frac{1}{2}A_0(1 + \lambda), \quad (2a)$$

where $\lambda = \frac{bV_0}{aA_0} \in (-1, 0)$ and $A_0 = 4\pi r^2(1)$ is the surface area of a single particle. Therefore, the base radius and the volume of the spherical cap is solved and expressed as follows:

$$r_\delta = r_0\sqrt{(1 - \lambda^2)}, \quad (2b)$$

$$V_\delta = \frac{\pi}{3}r_0^3(2 - \lambda)(1 + \lambda)^2, \quad (2c)$$

where $r_0 = r(1)$ is the radius of the single particle. The height of the preadsorption activated crystal at transition state of the ($n \rightarrow n + 1$) forward reaction is denoted by the function $h(n)$, which is defined through the following equation:

$$\frac{\pi}{6}h(3r_\delta^2 + h^2) = V_0n + V_\delta. \quad (3)$$

The activation energy is the free energy difference between the transition state and the ground state, so in the forward reaction, it is determined by the change of total interfacial area associated with the preadsorption activation:

$$\Delta G_+^*(n) = aA_+ + a\pi[h^2(n) - 4r^2(n)], \quad (4a)$$

where $A_+ = A_\delta + \pi r_\delta^2$. Following the same procedure, the activation energy of the backward reaction is solved as follows:

$$\Delta G_-^*(n) = aA_- + a\pi[h^2(n-1) - 4r^2(n)], \quad (4b)$$

where $A_- = A_0 - A_\delta + \pi r_\delta^2$. We plot the n -dependent activation energies ΔG_\pm^* for forward and backward reactions in Fig. 1(c). The critical size effect is manifested when n approaches n_c . When n is smaller than the critical value, the forward activation energy is higher than the backward, which indicates that a small cluster is thermodynamically favored. This shows that the birth of small nanocrystals is driven by fluctuation rather than thermodynamic force. At the critical size, the forward and backward reactions are balanced with the identical activation energies. After n becomes larger than n_c , the forward activation energy becomes smaller than the backward, and the continuous growth of large crystals is driven by thermodynamic force.

Based on the equations of ground-state free energy and activation energy, we analyze the convergence and asymptotic behaviors of several functions. (See the Appendix for a detailed derivation). It is shown that (1) the ground-state free energy profile converges to local flat geometry in a $-1/3$ -power law as n increases; (2) the activation energy converges to constant in a similar way; (3) the forward-backward activation difference, $\Delta G_+^*(n) - \Delta G_-^*(n)$, converges to the ground-state free energy gap, $G(n) - G(n-1)$, in a $-4/3$ -power law. These asymptotic behaviors of free energy

landscape are crucial to the crystal growth at long times and will be further addressed in the following sections.

B. Stochastic nucleation-growth dynamics of chain reactions

MCSs have been widely applied among topics in statistical physics [37–39], especially in the stochastic diffusion kinetics during phase transition where other methods, such as molecular dynamics simulation, were not feasible for long-time simulations [40,41]. Since the early 1990s, the development of kinetic MCSs has inspired the dynamic simulations for crystal growth [42–44], but the previous works have been mostly built on the ground-state free energy profiles and missed the transition states in the reaction mechanism [45–48]. Thus, the activation-adsorption-relaxation pathway enables us to overcome this disadvantage with the activated free energy landscape as an extension of classical theories. Based on the activation energy, we conduct the MCS for the stochastic chain reactions of the crystallization process. The forward or backward reaction probability is calculated as follows:

$$w_\pm(n) = \frac{1}{2}e^{-\Delta G_\pm^*(n)/k_B T}, \quad (5)$$

where $\Delta G_\pm^*(n)$ is the activation energy of forward or backward reaction. The details of the simulation algorithm are presented in the Appendix.

The MCS results unveil the distinct crystallization stages at various time scales. We plot the dynamic evolution of the mean volume $\langle n \rangle$ and mean radius $\langle r \rangle$ of the nanocrystals in Fig. 2(a). The crystallization process is separated into two stages: prenucleation and postnucleation. The prenucleation stage describes the early development of small nanocrystals before they reach the critical size. A transient slowdown is denoted by the intermediate plateau of the growth curve. Afterwards, nucleation events occur and lead to the transition towards the postnucleation stage.

At the beginning of the prenucleation stage, the evolution reflects the birth dynamics of nanocrystals from the initial system without any crystal denoted as $n = 0$. The subsequent enlargement is hindered by the dominant backward reaction probability w_- , as it is larger than the forward reaction probability w_+ , leading to the slowing down of the prenucleation growth. Around the slowdown regime, a quasiequilibrium state is reached, where the nanocrystals follow the Maxwell-Boltzmann distribution. At the quasiequilibrium state, the characteristic mean volume and radius are expressed as follows:

$$\bar{n}_c = \frac{1}{Z} \sum_{n=0}^{n_c} n e^{-G(n)/k_B T}, \quad (6a)$$

$$\bar{r}_c = \frac{1}{Z} \sum_{n=0}^{n_c} r e^{-G(n)/k_B T}, \quad (6b)$$

where $Z = \sum_{n=0}^{n_c} e^{-G(n)/k_B T}$. These values characterize the quasiequilibrium limit of the prenucleation stage and play the role of the threshold for the nucleation events.

After entering the postnucleation stage, the nanocrystals continue to grow. At the beginning of the postnucleation stage, the nucleation events promote crystallization with the emergent large crystals of volume larger than n_c . In the late postnucleation stage where $\langle n \rangle \gg n_c$, the growth rate

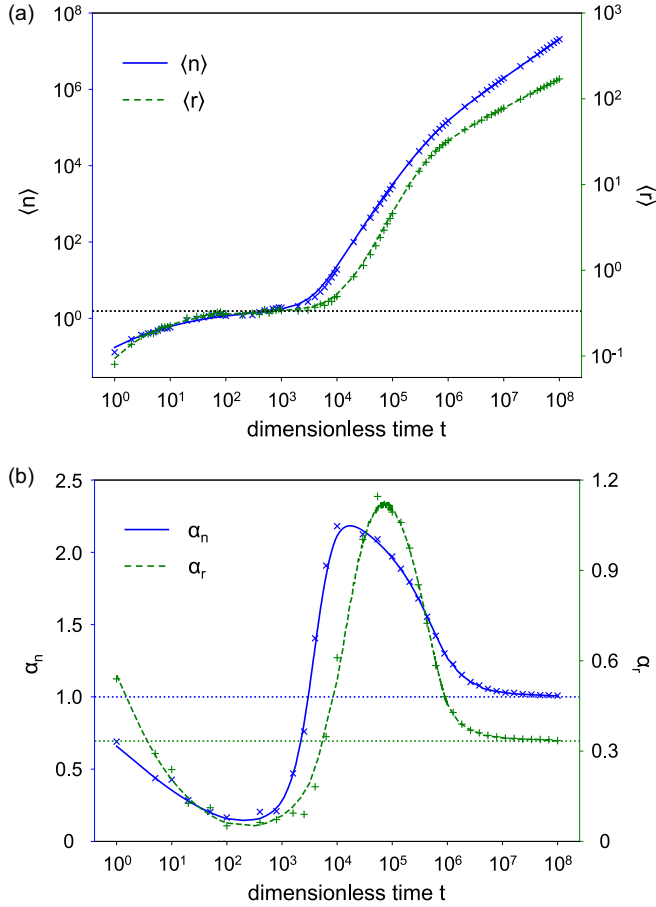


FIG. 2. Time-resolved evolution of the nucleation-growth dynamics. The curves denote the numerical solutions of ME and FPE. The markers show the results of MCS. (a) Mean crystal volume and mean crystal radius versus time. The horizontal line denotes \bar{n}_c and \bar{r}_c at quasiequilibrium. (b) Dynamic growth exponents based on mean volume and mean radius versus time. The upper and lower horizontal lines respectively denote the asymptotic limits as $\alpha_n \rightarrow 1$ and $\alpha_r \rightarrow 1/3$.

becomes stable because the activation energies converge towards n -independent constants. As a result, a crossover from superlinear- to linear-growth regimes is observed in the post-nucleation stage. To characterize this dynamic crossover, we define the time-resolved growth exponents based on the time-resolved evolution of mean crystal volume and radius in the logarithmic scale as $\alpha_n = d \ln \langle n \rangle / d \ln t$ and $\alpha_r = d \ln \langle r \rangle / d \ln t$ [Fig. 2(b)]. In the superlinear regime right after the transition from pre- to postnucleation growth, α_n is larger than 1. In the linear regime at long times, α_n converges towards 1, indicating a linear growth of the nanocrystal volume as time passes.

To model the nucleation-growth dynamics in the continuous-time fashion and explicate the evolution of the probability distribution, we use the following ME to describe the stochastic kinetics of the chain reactions:

$$\frac{\partial p(n, t)}{\partial t} = \sum_{n'=0}^{+\infty} [K_{n,n'} p(n', t) - K_{n',n} p(n, t)], \quad (7)$$

where $p(n, t)$ is the time-dependent probability density function and $K_{n,n'}$ is the transition operator for the reaction-induced transition from n' to n . According to the reaction mechanism, only single-particle exchange is considered, so K forms a sparse transition matrix whose off-diagonal terms are shown as follows:

$$K_{n+1, n} = k_+ e^{-\Delta G_+^*/k_B T}, \quad (8a)$$

$$K_{n-1, n} = k_- e^{-\Delta G_-^*/k_B T}, \quad (8b)$$

where k_{\pm} is the reaction prefactor that characterizes the basic reaction frequency of forward or backward reaction. With a transform of $\Delta G_+^* \rightarrow \Delta G_+^* + k_B T \ln \frac{k_+}{k_-}$ and $\Delta G_-^* \rightarrow \Delta G_-^* + k_B T \ln \frac{k_-}{k_+}$, we could unify the prefactor in a symmetric form as $k = \sqrt{k_+ k_-}$. The numerical solution of ME extends the results of MCS in a continuous-time fashion and further provides the evolution dynamics of probability distribution.

In the prenucleation stage [Fig. 3(a)], the probability density function evolves from the initial condition of a delta function to the quasiequilibrium where $p \propto \exp[-G(n)/k_B T]$. During the continuous broadening of the probability density function, the small- n part is almost conserved, while the large- n tail gets boosted slowly. It is a nonequilibrium relaxation driven by fluctuation that counterbalances the thermodynamical driving force $-\nabla_n G$ favoring a diminishing nanocrystal when $n < n_c$. Such a negative thermodynamical force impedes the propagation of the probability density function at the large- n tail, and the small- n region is allowed to approach transient detailed balance at the quasiequilibrium limit of the prenucleation stage where $\langle n \rangle = \bar{n}_c$.

Then, the postcritical crystals start to emerge and thus nucleation events begin. During the nucleation, the probability density function shows a transition from the monotonic to bimodal pattern [Fig. 3(b)]. At the small- n region, despite the stability of the curvature that indicates the preserved local quasiequilibrium, the probability drops significantly with time. At the large- n region, not only is the fast tail propagation observed, but a second peak also emerges and rises, illustrating the nucleation of the large nanocrystals beyond n_c . This transition reflects Ostwald's ripening that describes the generation of large crystalline clusters through the thermodynamically disfavored intermediates.

Apart from the monotonic-bimodal transition of the probability density function, the nucleation dynamics is also characterized by an exponential decay of the small nanocrystals [Fig. 3(c)]. Elicited from MCS and ME results, the phenomenological equation of nucleation process could be written as follows:

$$P_0 = e^{-k_N t}, \quad (9)$$

where $P_0 = \sum_{n=0}^{n_c} p(n, t)$ is the cumulative probability of the nanocrystals that are smaller than or equal to the critical size, and k_N is the nucleation rate. With k_N , crystallization is characterized as a multistage process across the corresponding time scales. When $t \ll k_N^{-1}$, nucleation events have not started and P_0 almost remains stationary as 1, indicating the prenucleation stage. When $t \approx k_N^{-1}$, the emergence of crystals beyond the critical size denotes the early postnucleation stage,

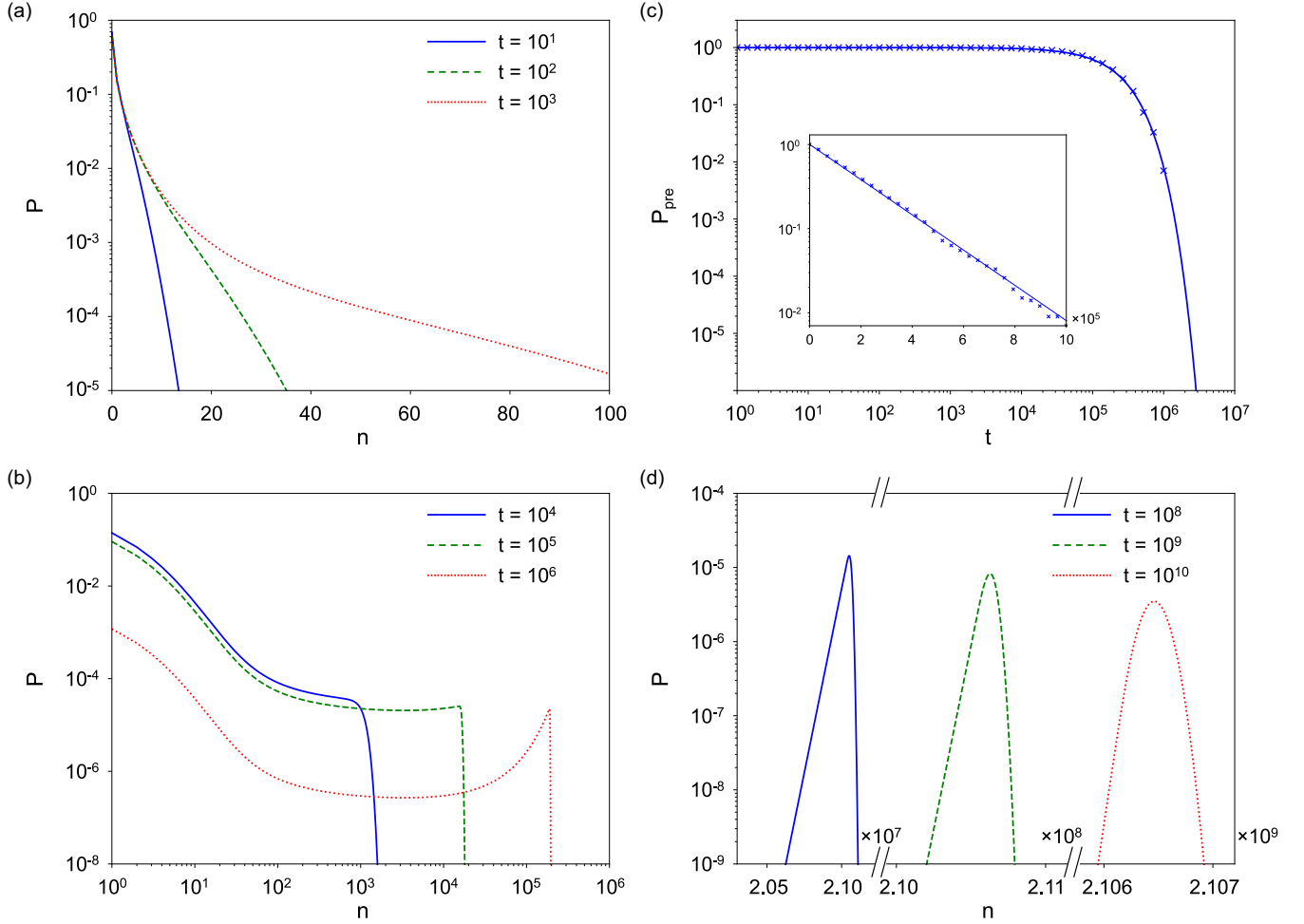


FIG. 3. The probability density functions at different crystallization stages. (a) Prenucleation stage. (b) Transition from prenucleation to early postnucleation stage. (c) Exponential decay of small clusters during nucleation. The solid lines denote the numerical solutions of ME and FPE. The markers show the results of MCS. (d) Late postnucleation stage.

whereas $t \gg k_N^{-1}$ implies the end of nucleation events and the late postnucleation stage. Based on the numerical results, we extract the value of k_N and compare it with previous studies. Evaluation of k_N with the nucleation rate from the classical nucleation theory gives a Zeldovich factor of around 10^{-3} – 10^{-2} , consistent with experiments and simulations of the liquid-phase crystallization [49,50]. Besides, k_N is of the same order of magnitude as the Kramers escape rate but is around twofold smaller [51]. This difference will be explained with the Fokker-Planck formalism in the next section.

After nucleation, the small- n region of the probability density function decays and the large- n region dominates the statistics. The probability density function is a moving mixture of exponential and Gaussian components, and the net propagation is driven by the gradient of free energy profile. The exponential component is associated with the nucleation dynamics and the Gaussian component is related to the stochastic fluctuation, which will be explained in the next section as well.

C. Fokker-Planck formalism of nucleation-growth dynamics as heterogeneous random walk

In this paper, the activation energies are expressed through differentiable functions, so the ME could be formulated in the Fokker-Planck fashion when n is a continuous variable (see the Appendix). The corresponding FPE is written as follows:

$$\frac{\partial p(n, t)}{\partial t} = \frac{\partial}{\partial n} D_1 p + \frac{\partial^2}{\partial n^2} D_2 p, \quad (10a)$$

where

$$D_1 = 2k e^{-[\Delta G_+^*(n) + \Delta G_-^*(n)]/2k_B T} \sinh \frac{\Delta G_+^*(n) - \Delta G_-^*(n)}{2k_B T}, \quad (10b)$$

$$D_2 = k e^{-[\Delta G_+^*(n) + \Delta G_-^*(n)]/2k_B T} \cosh \frac{\Delta G_+^*(n) - \Delta G_-^*(n)}{2k_B T}. \quad (10c)$$

The two terms on the right-hand side of Eq. (10a) denote the drift and diffusion components of the FPE respectively. Equation (10a) is equivalent to the following stochastic differential equation for the generalized Langevin dynamics:

$$\frac{dn}{dt} = -\frac{k}{k_B T} \nabla_n F + \sqrt{D_2} \xi, \quad (11a)$$

where ξ is a Gaussian white noise, and F is defined as follows:

$$F = \frac{k_B T}{k} \int_0^n D_1 dn. \quad (11b)$$

Hence, we describe the nucleation-growth process as a heterogenous random walk. Since D_1 denotes the reaction-induced driving force as a function of ΔG_{\pm}^* , F is the potential function characterizing the activated free energy landscape. Besides, the explicit n dependence of D_2 demonstrates the heterogeneity of the diffusion term and induces a spurious drift. These features help to explain the discrepancy between the nucleation rate k_N and the Kramers escape rate. The potential function depicted by F does not have parabolic behaviors at its local extremes, in contrast to the condition used in Kramers' derivation, leading to high-order corrections that reduce the escape rate [51]. Also, D_2 varies with n , which is different from the state-independent diffusion constant in Kramers' calculation.

However, the heterogeneous effect decays as n increases. From the analysis of the asymptotic behaviors of the activation energy, it is shown that the ground-state free energy tends to a constant-gradient flat geometry, and the forward and backward activation energies converge to two constants, when the crystal size approaches infinity. The related convergence could be described by a 1/3-power law. In such a limit, D_1 and D_2 becomes n independent, so Eqs. (10a) and (11a) describe a simple random walk. This scenario is consistent with the linear-growth regime in the late postnucleation stage, and the corresponding dynamics could be simplified as follows:

$$\frac{d\langle n \rangle}{dt} = -\frac{kb}{k_B T} e^{-a(A_0 - 2\pi r_0^2)/2k_B T}. \quad (12)$$

Since D_1 and D_2 converge to constants in the linear-growth regime, the transition probability of FPE turns out to be a Gaussian kernel. The probability density function could be expressed as the convolution of the Gaussian kernel and the nucleation dynamics:

$$p = - \int_0^t \frac{1}{\sqrt{4\pi D_2(t-\tau)}} e^{-[n-n_c+D_1(t-\tau)]^2/4D_2(t-\tau)} \frac{dP_0(\tau)}{d\tau} d\tau. \quad (13)$$

This equation explains the postnucleation probability density function shown in Fig. 3(d). The left part of probability density function depicts an exponential behavior because of P_0 [Eq. (9)], and the right part is a Gaussian tail with the variance of $2D_2 t$. Over time, while the exponential component remains stable, the Gaussian component undergoes broadening, resulting in the long-time probability density function converging towards a simple Gaussian curve.

Moreover, we examine the robustness of the power-law relations between the mean volume and radius of the nanocrystals in the postnucleation stage. In general, $3\alpha_r = \alpha_n$ does not always hold for an arbitrary probability density

function, because this equality requires that $\langle r \rangle^3 \propto \langle n \rangle$, which breaks down due to the nonequilibrium heterogeneous random walk at the prenucleation stage and the bimodality behavior during nucleation. However, there are two specific regimes where $3\alpha_r = \alpha_n$ is preserved: the quasiequilibrium limit of the prenucleation stage and the late postnucleation stage where $\langle n \rangle \gg n_c$. During the transient quasiequilibrium, the growth of the nanocrystals pauses, so both α_r and α_n are close to zero. On the other hand, when the postnucleation linear-growth regime is approached, $4\pi \langle r \rangle^3 = 3\langle n \rangle$, so that $\alpha_r = 1/3$ and $\alpha_n = 1$ (see the Appendix for the detailed derivation).

D. Scale effect in collision frequency and activation relaxation steps

In previous sections, we studied the nucleation-growth dynamics based on the stochastic chain reactions with the assumption that the dilute solution remains constant. This is consistent with the situation of the early development of nanocrystals where only small crystalline clusters are formed and most particles stay in the solution phase. Under this circumstance, the reaction kinetics follows the mass action law and is determined by the activation energies and the concentrations of different components, while the prefactor k is independent of the volume or radius of nanocrystals. However, when the crystals keep growing, especially in the late postnucleation stage where the crystal radius approaches one hundred nanometers or even beyond one micrometer, the scale effect starts to play an important role in modifying the collision frequency [52]. When the crystal radius is at the same scale as the average interparticle distance in the solution, the crystal could not be treated as a volumeless point, and the collision frequency is no longer a simple product of the concentrations, because the scattering cross section scales with the crystal size. Besides, the scale effect would also affect the activation and relaxation time along the reaction pathway. Since the activation and relaxation steps characterize reorganizations of the crystal conformation driven by fluctuation dissipation, their rates also vary with the crystal size. For a small nanocrystal, the activation and relaxation time is negligible, so k is simply determined by the collision frequency. But for a large crystal, the reorganization time enlarges and slows down the overall reaction kinetics.

These factors invoke a generalization of the model for large-crystal growth with a scale-dependent k . Hence, we extend the model with a radius-dependent k as follows:

$$k \sim r^\beta. \quad (14)$$

Since this scale effect is significant for large crystals in the late postnucleation stage where the growth dynamics follows a characteristic power-law relation, the corresponding power law is extended as follows:

$$\langle r \rangle \propto t^{\alpha'_r} = t^{\alpha_r/(1-\alpha_r\beta)}. \quad (15)$$

This equation broadens the spectrum of the power exponent from the scenario of a constant k to that of a scale-dependent k . In the trivial case of $\beta = 0$, we restore the simple relation of $\alpha'_r = \alpha_r = 1/3$. If the collision between the spherical crystal and solute particles is the rate-limiting mechanism, $\beta = 2$ and $\alpha'_r = 1$. On the condition that the

activation and relaxation dynamics follows a heat diffusion equation, we have $\beta = 1$ and $\alpha'_r = 1/2$, consistent with the classical solution of the one-phase Stefan problem [53,54] and the reaction-limited solution of LSW model [11,12].

III. DISCUSSION

The activation-adsorption-relaxation pathway provides a detailed depiction of the evolution of free energy along the reaction coordinate. This pathway aids in formulating the reaction kinetics by utilizing the activation energy from the transition-state configuration, and in turn, sheds light on the underlying physicochemical mechanism that underpins the interplay between crystal growth kinetics and transient structural reorganization. The intermediate transition states extend the ground-state free energy profile with the activated conformations induced by fluctuation. Our utilization of the activation-adsorption-relaxation mechanism allows us to model the elementary reaction events via transition state theory. Furthermore, by computing the size-dependent activation energy, we account for a crucial aspect that has been overlooked in classical nucleation-growth theories. Previous works, such as the Wilson-Frenkel, BD, and LSW models [7,8,10–12], commonly estimated nucleation kinetics based solely on ground-state free energy, neglecting the crucial role of activation energy in nonequilibrium processes across reaction barriers. By incorporating the activated free energy landscape, our approach provides a more complete and nuanced understanding of crystallization dynamics from a reaction-centric viewpoint, thereby potentially reconciling discrepancies between experimental findings and classical theoretical models. The size-dependent activation energies contribute to the heterogeneity of the stochastic reaction kinetics, as an extension of diffusion models for varying power laws [32,33]. This scenario remained obscure until the recent development of experimental and simulation techniques. The state-of-art electron microscopy and NMR methods have enabled the time-resolved measurements of crystal growth with subnanometer resolution, and the evolution of the structural heterogeneity has been observed during the early development of the small nanocrystals [28,29,55]. Thus, the theory reported in this work provides quantifiable relationships that can be verified in future experiments and simulations [19,20].

Our quantitative findings pertaining to the postnucleation stage exhibit high levels of generalizability across diverse systems, as evidenced by their agreement with a broad range of experimental and simulation studies. The exponential nucleation dynamics is in general consistence with previous measurements, and the nucleation rate calculated in our model extends the Kramers escape rate with heterogeneous effect. Besides, our model explains the different power-law relations during the late postnucleation growth. In an ideal dilute system, the mean crystal volume grows linearly with time, i.e., $\alpha_n = 1$. For spherical nanocrystals, α_r takes 1/3 for the reaction-based growth exponent. When the scale-dependent collision and activation-relaxation mechanisms are considered, we find $\alpha_r = 1/2$, which could be generalized to the system of any integer dimension. This result agrees with the classical solution of the multidimension one-phase Stefan problem and the reaction-limited solution of the LSW model

[11,12,53,54]. It has been observed in the reaction-limited growth of faceted nanoflakes [21] and liquid-liquid phase separation systems [22]. The growth exponent could be further reduced if the activation or relaxation is slow and plays the rate-limiting role. For instance, a power law of around 1/8 has been seen in the growth of spherical nanocrystals, indicating that the relaxation of crystal conformation is achieved through the stochastic reptation motion [21]. By this means, Eq. (15) broadens the power-law relations for different dimensions and scale-dependent relaxation, which could explain the diverse growth exponents observed in various systems. Moreover, the transient superlinear regime at the beginning of the postnucleation growth displays a dynamic feature that has not been studied and invokes future endeavors.

Given that our model describes the nucleation-growth dynamics of individual nanocrystals in an ideal constant solution, these results can be applied to open systems coupled with well-controlled baths, provided that the solute concentration remains higher than that of the nanocrystals. Nevertheless, it is worth noting that as the crystal radii approach hundreds of nanometers or even exceed one micrometer, the majority of solute particles have already crystallized. Hence, the further crystallization process is driven by the coalescence of multiple crystals, resulting in a reduction in the total number of individual nanocrystals [52]. Likewise, in a closed finite-size system, particularly during spontaneous homogeneous nucleation, our model is solely applicable for elucidating the early stages of crystallization, i.e., the prenucleation stage. This is because during the late-stage development of large crystals in a closed system, the coalescence of multiple crystals becomes the dominant process instead of solute adsorption, as the solute concentration is relatively low and crystal-crystal interactions assume greater significance.

ACKNOWLEDGMENTS

This work has been funded by Research Grants Council Collaborative Research Fund (Grant No. C7035-20G), HKUST Grant (Grant No. R9418), the Project of Hetao Shenzhen-Hong Kong Science and Technology Innovation Cooperation Zone (Grant No. HZQB-KCZYB-2020083), and the Society of Interdisciplinary Research (SOIRÉE).

APPENDIX

1. Convergence of $G(n)$ and $\Delta G_{\pm}^*(n)$

We analyze the convergence of several important functions based on the ground-state free energy and activation energy from Eqs. (1) and (4). Here, we show the derivations.

(i) $\Delta G(n) = G(n) - G(n-1)$: Substituting the expression of the ground-state free energy in Eq. (1), we get

$$\Delta G(n) = a\sqrt[3]{36\pi V_0^2 [n^{2/3} - (n-1)^{2/3}] + bV_0}. \quad (\text{A1})$$

The terms in the bracket on the right-hand side of Eq. (A1) could be expressed as follows:

$$n^{2/3} - (n-1)^{2/3} = \frac{2}{3} \int_{n-1}^n x^{-1/3} dx. \quad (\text{A2})$$

Because $n^{-1/3} < \int_{n-1}^n x^{-1/3} dx < (n-1)^{-1/3}$, $\Delta G(n) - bV_0$ converges to 0 faster than $\frac{2a}{3}\sqrt[3]{36\pi V_0^2/(n-1)}$. In other words, the ground-state free energy profile shows $(-1/3)$ -power-law convergence to a local flat geometry.

(ii) $\Delta G_{\pm}^*(n)$: From Eq. (3), the height of the transition-state crystal is solved as follows:

$$h(n) = p(n) - \frac{r_{\delta}^2}{p(n)}, \quad (\text{A3a})$$

where

$$p(n) = \sqrt[3]{\frac{1}{2}[\sqrt{4r_{\delta}^6 + q^2(n)} + q(n)]}, \quad (\text{A3b})$$

$$q(n) = 8r^3(n) + \frac{6}{\pi}V_{\delta}. \quad (\text{A3c})$$

Substituting Eq. (2), we find that p is monotonically increasing with respect to $\lambda \in (-1, 0)$, and thus $2r(n) < p(n) < 2r(n+1)$. We define the function σ as

$$\sigma(x, y) = h^2(x) - 4r^2(y) + 2r_{\delta}^2. \quad (\text{A4})$$

As a result, we have the following inequalities:

$$\frac{r_{\delta}^4}{16r^2(n+1)} < \frac{\sigma(n, n)}{4} < r^2(n+1) - r^2(n) + \frac{r_{\delta}^4}{16r^2(n)}, \quad (\text{A5a})$$

$$r^2(n-1) - r^2(n) < \frac{\sigma(n-1, n)}{4} < \frac{r_{\delta}^4}{16r^2(n-1)}. \quad (\text{A5b})$$

With the same procedure for the convergence of $G(n) - G(n-1)$, we see that $\sigma(n, n)$ and $\sigma(n-1, n)$ both show $(-1/3)$ -power-law convergence towards zero as $n \rightarrow +\infty$. Together with Eqs. (4), it indicates that both forward and backward activation energies follow the same type of convergence towards their $n \rightarrow +\infty$ limits:

$$\lim_{n \rightarrow +\infty} \Delta G_{+}^*(n) = a(A_{\delta} - \pi r_{\delta}^2), \quad (\text{A6a})$$

$$\lim_{n \rightarrow +\infty} \Delta G_{-}^*(n) = a(A_0 - A_{\delta} - \pi r_{\delta}^2). \quad (\text{A6b})$$

(iii) We define the function $\psi(n) = [\Delta G_{+}^*(n) - \Delta G_{-}^*(n)] - [G(n) - G(n-1)]$, and based on Eq. (A4), it could be expressed in terms of σ function as follows:

$$\psi(n) = a\pi[\sigma(n, n) - \sigma(n-1, n-1)]. \quad (\text{A7})$$

Since $\sigma(n, n) - \sigma(n-1, n-1) = \int_{n-1}^n \frac{d}{dn}\sigma(n, n)dn$, we get the inequality $a\pi \inf\{\frac{d}{dx}\sigma(x, x) : x \in [n-1, n]\} < \psi(n) < a\pi \sup\{\frac{d}{dx}\sigma(x, x) : x \in [n-1, n]\}$. Therefore, σ contributes to the $(-4/3)$ -power-law convergence of ψ so that $\Delta G_{+}^*(n) - \Delta G_{-}^*(n)$ converges towards $G(n) - G(n-1)$ in the same way.

2. Monte Carlo simulation algorithm

Throughout the chain reactions, each elementary reaction is modeled as a stochastic single-particle exchange event between the solution and crystal phases. The overall chain reactions of the nucleation-growth process start with the initial condition denoted by $n = 0$, where no crystal exists, i.e., all crystals are in a trivial state of zero volume. The forward and

backward transition probabilities between $n = 0$ and $n = 1$ are calculated from the ground-state free energy gap instead of the activation energies, and all other transition probabilities are calculated from ΔG_{\pm}^* . The basic simulation procedure follows the Metropolis-Hastings algorithm [37–39]. We conduct 1000 simulation runs, each of 2×10^8 time steps.

3. Parameter values in numerical methods

In this study, all the parameters and variables are set as unitless quantities in numerical methods, including MCS and numerical solutions of ME and FPE. The unit volume is set as the volume of a single particle, i.e., $V_0 = 1$. The radius is calculated from the unitless volume. The unitless time in ME and FPE equals the index of the corresponding time step in MCS. The transition probabilities between the 0 and 1 state are determined by the ground-state free energy gap, while others are calculated from ΔG_{\pm}^* . The scale-independent k is assigned 1. The values of other physical parameters are shown as follows: $k_B = 1$, $T = 3$, $a = 1.1$, and $b = -1.0$.

4. Derivation of Fokker-Planck equation

From Eqs. (7) and (8), we have the form of the ME as follows:

$$\begin{aligned} \frac{\partial p(n, t)}{k \partial t} &= e^{-\Delta G_{+}^*(n-1)/k_B T} p(n-1, t) \\ &+ e^{-\Delta G_{-}^*(n+1)/k_B T} p(n+1, t) \\ &- [e^{-\Delta G_{-}^*(n)/k_B T} + e^{-\Delta G_{+}^*(n)/k_B T}] p(n, t). \end{aligned} \quad (\text{A8})$$

After substituting the expression of Eqs. (10b) and (10c), we get

$$\begin{aligned} \frac{\partial P(n, t)}{\partial t} &= [D_2(n-1)P(n-1, t) - 2D_2(n)P(n, t) \\ &+ D_2(n+1)P(n+1, t)] \\ &+ \frac{1}{2}[D_1(n+1)P(n+1, t) - D_1(n-1)P(n-1, t)]. \end{aligned} \quad (\text{A9})$$

Although ΔG_{\pm}^* are originally defined as the forward and backward activation energies for discrete states of integer n , their explicit forms are expressed by differentiable functions, so they could be directly generalized to differentiable functions as well as D_1 and D_2 . When n is a continuous variable, the first term on the right-hand side of Eq. (A9) is equivalent to $\frac{\partial^2}{\partial n^2} D_2(n)P(n, t)$ and the last term is equivalent to $\frac{\partial}{\partial n} D_1(n)P(n, t)$. In other words, Eq. (10a) is a generalized partial differential equation from Eq. (7) in the continuous- n limit.

5. Mean volume and mean radius in the linear-growth regime

In the continuous limit, the mean values of n and r are calculated as follows:

$$\langle n \rangle = \int_0^{+\infty} n p(n, t) dn, \quad (\text{A10a})$$

$$\langle r \rangle = \int_0^{+\infty} \sqrt[3]{\frac{3n}{4\pi}} p(n, t) dn. \quad (\text{A10b})$$

In the late postnucleation stage, the probability density function follows Eq. (13), and since $D_1 t \gg n_c$, we have

$$\langle r \rangle = \int_0^t \int_0^{+\infty} \sqrt[3]{\frac{3n}{4\pi}} e^{-[n+D_1(t-\tau)]^2/4D_2(t-\tau)} \times \frac{k_N e^{-k_N \tau}}{\sqrt{4\pi D_2(t-\tau)}} dn d\tau. \quad (\text{A11})$$

The integration of n could be solved by the following relation:

$$\int_0^\infty \sqrt[3]{n} e^{-(n-y)^2/x} dn = \frac{x^{2/3}}{2} \Gamma\left(\frac{2}{3}\right) f\left(-\frac{1}{6}; \frac{1}{2}; \frac{y^2}{-x}\right) + y \sqrt[6]{x} \Gamma\left(\frac{7}{6}\right) f\left(\frac{1}{3}; \frac{3}{2}; \frac{y^2}{-x}\right), \quad (\text{A12})$$

where f is the Kummer confluent hypergeometric function, $x = 4D_2(t-\tau)$, and $y = -D_1(t-\tau)$. Because $y^2 \gg x$ at large times, we conduct series expansion of f at infinity and keep

the nonvanishing terms:

$$\lim_{y^2/x \rightarrow \infty} \int_0^\infty \sqrt[3]{n} e^{-(n-y)^2/x} dn = \sqrt{\pi x y^{1/3}}. \quad (\text{A13})$$

Substituting Eq. (A13) into Eq. (A11), we get the expression as follows:

$$\langle r \rangle = \sqrt[3]{-\frac{3D_1}{4\pi}} \int_0^t k_N e^{-k_N \tau} (t-\tau)^{1/3} d\tau. \quad (\text{A14})$$

The integration of τ involves a Gamma function and an exponential integral. Because at the large times, $t \gg k_N^{-1}$, we also conduct series expansion of the exponential integral at infinity and keep the largest nonvanishing term:

$$\langle r \rangle = \sqrt[3]{-\frac{3D_1 t}{4\pi}}. \quad (\text{A15})$$

Following the same procedure, we calculate $\langle n \rangle$ and get the closed-form expression as follows:

$$\langle n \rangle = -D_1 t. \quad (\text{A16})$$

As a result, the equality $4\pi \langle r \rangle^3 = 3 \langle n \rangle$ is preserved in the late postnucleation stage.

-
- [1] N. T. K. Thanh, N. Maclean, and S. Mahiddine, Mechanisms of nucleation and growth of nanoparticles in solution, *Chem. Rev.* **114**, 7610 (2014).
- [2] S. Karthika, T. K. Radhakrishnan, and P. Kalaichelvi, A Review of classical and nonclassical nucleation theories, *Cryst. Growth Des.* **16**, 6663 (2016).
- [3] Y.-S. Jun, Y. Zhu, Y. Wang, D. Ghim, X. Wu, D. Kim, and H. Jung, Classical and nonclassical nucleation and growth mechanisms for nanoparticle formation, *Annu. Rev. Phys. Chem.* **73**, 453 (2022).
- [4] P. W. Voorhees, The theory of ostwald ripening, *J. Stat. Phys.* **38**, 231 (1985).
- [5] J. A. Marqusee and J. Ross, Theory of ostwald ripening: Competitive growth and its dependence on volume fraction, *J. Chem. Phys.* **80**, 536 (1984).
- [6] J. H. Yao, K. R. Elder, H. Guo, and M. Grant, Theory and simulation of ostwald ripening, *Phys. Rev. B* **47**, 14110 (1993).
- [7] H. W. Wilson, On the velocity of solidification and viscosity of super-cooled liquids, *Philos. Mag. (1798-1977)* **50**, 238 (1900).
- [8] J. Frenkel, Note on a relation between the speed of crystallization and viscosity, *Phys. Z. Sowjetunion* **1**, 498 (1932).
- [9] H. Vehkamäki, *Classical Nucleation Theory in Multicomponent Systems* (Springer, Berlin, 2006).
- [10] R. Becker and W. Döring, Kinetische behandlung der keimbildung in übersättigten dämpfen, *Ann. Phys.* **416**, 719 (1935).
- [11] I. M. Lifshitz and V. V. Slyozov, The kinetics of precipitation from supersaturated solid solutions, *J. Phys. Chem. Solids* **19**, 35 (1961).
- [12] C. L. Wagner, Theorie Der Alterung von niederschlägen durch umlösen (ostwald-reifung), *Z. Elektrochem.* **65**, 581 (1961).
- [13] O. Penrose, The becker-döring equations at large times and their connection with the lsw theory of coarsening, *J. Stat. Phys.* **89**, 305 (1997).
- [14] J. J. L. Velázquez, The becker-döring equations and the lifshitz-slyozov theory of coarsening, *J. Stat. Phys.* **92**, 195 (1998).
- [15] P. Laurençot and S. Mischler, From the becker-döring to the lifshitz-slyozov-wagner equations, *J. Stat. Phys.* **106**, 957 (2002).
- [16] F. Celestini and J.-M. Debierre, Measuring kinetic coefficients by molecular dynamics simulation of zone melting, *Phys. Rev. E* **65**, 041605 (2002).
- [17] A. Kerrache, J. Horbach, and K. Binder, Molecular-dynamics computer simulation of crystal growth and melting in Al50Ni50, *Europhys. Lett.* **81**, 58001 (2008).
- [18] D. Alloyeau, G. Prévot, Y. Le Bouar, T. Oikawa, C. Langlois, A. Loiseau, and C. Ricolleau, Ostwald Ripening in Nanoalloys: When Thermodynamics Drives a Size-Dependent Particle Composition, *Phys. Rev. Lett.* **105**, 255901 (2010).
- [19] R. Freitas and E. J. Reed, Uncovering the effects of interface-induced ordering of liquid on crystal growth using machine learning, *Nat. Commun.* **11**, 3260 (2020).
- [20] P. A. Santos-Florez, H. Yanxon, B. Kang, Y. Yao, and Q. Zhu, Size-Dependent Nucleation in Crystal Phase Transition from Machine Learning Metadynamics, *Phys. Rev. Lett.* **129**, 185701 (2022).
- [21] T. J. Woehl, J. E. Evans, I. Arslan, W. D. Ristenpart, and N. D. Browning, Direct in situ determination of the mechanisms controlling nanoparticle nucleation and growth, *ACS Nano* **6**, 8599 (2012).
- [22] J. Colombani and J. Bert, Toward a complete description of nucleation and growth in liquid-liquid phase separation, *J. Non-Equilibrium Thermodyn.* **29**, 389 (2004).
- [23] M. N. van der Linden, L. C. Alexander, D. G. A. L. Aarts, and O. Dauchot, Interrupted Motility Induced Phase Separation in Aligning Active Colloids, *Phys. Rev. Lett.* **123**, 098001 (2019).

- [24] H. Zheng, R. K. Smith, Y. Jun, C. Kisielowski, U. Dahmen, and A. P. Alivisatos, Observation of single colloidal platinum nanocrystal growth trajectories, *Science* **324**, 1309 (2009).
- [25] J. M. Grogan, L. Rotkina, and H. H. Bau, In Situ liquid-cell electron microscopy of colloid aggregation and growth dynamics, *Phys. Rev. E* **83**, 061405 (2011).
- [26] Q. Chen, J. M. Yuk, M. R. Hauwiler, J. Park, K. S. Dae, J. S. Kim, and A. P. Alivisatos, Nucleation, growth, and superlattice formation of nanocrystals observed in liquid cell transmission electron microscopy, *MRS Bull.* **45**, 713 (2020).
- [27] W. Dachraoui, T. R. Henninen, D. Keller, and R. Erni, Multi-step atomic mechanism of platinum nanocrystals nucleation and growth revealed by in-situ liquid cell STEM, *Sci. Rep.* **11**, 23965 (2021).
- [28] J. Zhou, Y. Yang, Y. Yang, D. S. Kim, A. Yuan, X. Tian, C. Ophus, F. Sun, A. K. Schmid, M. Nathanson, H. Heinz, Q. An, H. Zeng, P. Ercius, and J. Miao, Observing crystal nucleation in four dimensions using atomic electron tomography, *Nature (London)* **570**, 500 (2019).
- [29] F.-R. Chen, D. Van Dyck, C. Kisielowski, L. P. Hansen, B. Barton, and S. Helveg, Probing atom dynamics of excited Co-Mo-S nanocrystals in 3D, *Nat. Commun.* **12**, 5007 (2021).
- [30] D. S. Grebenkov and L. Tupikina, Heterogeneous continuous-time random walks, *Phys. Rev. E* **97**, 012148 (2018).
- [31] E. Barkai, R. Metzler, and J. Klafter, From continuous time random walks to the fractional fokker-planck equation, *Phys. Rev. E* **61**, 132 (2000).
- [32] A. G. Cherstvy and R. Metzler, Population splitting, trapping, and non-ergodicity in heterogeneous diffusion processes, *Phys. Chem. Chem. Phys.* **15**, 20220 (2013).
- [33] K. Zhu and H. Su, Unraveling dynamic transitions in time-resolved biomolecular motions by a dressed diffusion model, *J. Phys. Chem. A* **124**, 613 (2020).
- [34] K. Zhu and H. Su, Generalization of langevin dynamics from spatio-temporal dressed dynamics perspective, *J. Phys. Chem. A* **124**, 3269 (2020).
- [35] R. A. Marcus, On the theory of oxidation-reduction reactions involving electron transfer. I, *J. Chem. Phys.* **24**, 966 (1956).
- [36] R. A. Marcus, On the theory of oxidation—reduction reactions involving electron transfer. v. comparison and properties of electrochemical and chemical rate constants I, *J. Phys. Chem.* **67**, 853 (1963).
- [37] N. Metropolis, A. W. Rosenbluth, M. N. Rosenbluth, A. H. Teller, and E. Teller, Equation of state calculations by fast computing machines, *J. Chem. Phys.* **21**, 1087 (1953).
- [38] W. K. Hastings, Monte carlo sampling methods using markov chains and their applications, *Biometrika* **57**, 97 (1970).
- [39] *Applications of the Monte Carlo Method in Statistical Physics*, edited by K. Binder (Springer, Berlin, 2013).
- [40] M. C. Bartelt and J. W. Evans, Scaling analysis of diffusion-mediated island growth in surface adsorption processes, *Phys. Rev. B* **46**, 12675 (1992).
- [41] M. Bott, M. Hohage, M. Morgenstern, T. Michely, and G. Comsa, New Approach for Determination of Diffusion Parameters of Adatoms, *Phys. Rev. Lett.* **76**, 1304 (1996).
- [42] K. A. Fichtorn and W. H. Weinberg, Theoretical foundations of dynamical Monte Carlo simulations, *J. Chem. Phys.* **95**, 1090 (1991).
- [43] M. Kotrla, Numerical simulations in the theory of crystal growth, *Comput. Phys. Commun.* **97**, 82 (1996).
- [44] A. C. Levi and M. Kotrla, Theory and simulation of crystal growth, *J. Phys.: Condens. Matter* **9**, 299 (1997).
- [45] L. Nurminen, A. Kuronen, and K. Kaski, Kinetic Monte Carlo simulation of nucleation on patterned substrates, *Phys. Rev. B* **63**, 035407 (2000).
- [46] A. F. Voter, F. Montalenti, and T. C. Germann, Extending the time scale in atomistic simulation of materials, *Annu. Rev. Mater. Res.* **32**, 321 (2002).
- [47] A. Filippini and P. Giammatteo, Kinetic Monte Carlo simulation of the classical nucleation process, *J. Chem. Phys.* **145**, 211913 (2016).
- [48] N. Cheimarios, D. To, G. Kokkoris, G. Memos, and A. G. Boudouvis, Monte Carlo and kinetic monte carlo models for deposition processes: A review of recent works, *Front. Phys.* **9**, 631918 (2021).
- [49] J. Y. Rempel, M. G. Bawendi, and K. F. Jensen, Insights into the kinetics of semiconductor nanocrystal nucleation and growth, *J. Am. Chem. Soc.* **131**, 4479 (2009).
- [50] D. Richard and T. Speck, Classical nucleation theory for the crystallization kinetics in sheared liquids, *Phys. Rev. E* **99**, 062801 (2019).
- [51] H. Risken, *The Fokker-Planck Equation: Methods of Solution and Applications*, 2nd ed. (Springer, Berlin, 1996).
- [52] V. Gimenez-Pinto, Ordering hard-sphere particle suspensions by medium crystallization: Effect of size and interaction strength, *Phys. Rev. E* **105**, L032601 (2022).
- [53] L. I. Rubenstein, *The Stefan Problem* (American Mathematical Society, Providence, Rhode Island, 1971).
- [54] A. M. Meirmanov, *The Stefan Problem* (De Gruyter, Berlin, Germany, 1992).
- [55] R. Mashiach, H. Weissman, L. Avram, L. Houben, O. Brontvein, A. Lavie, V. Arunachalam, M. Leskes, B. Rybtchinski, and A. Bar-Shir, In Situ NMR reveals real-time nanocrystal growth evolution via monomer-attachment or particle-coalescence, *Nat. Commun.* **12**, 229 (2021).